Microstrip Parallel-Coupled Filters With Cascade Trisection and Quadruplet Responses

Jhe-Ching Lu, Ching-Ku Liao, and Chi-Yang Chang, *Member, IEEE*

***Abstract*—Microstrip parallel-coupled filters with generalized Chebyshev responses are presented. The basic structure of the proposed filter is a conventional parallel-coupled filter of which the physical dimensions can be easily obtained by the well-known analytical method. With the aid of the equivalent circuit corresponding to a conventional parallel-coupled filter, the relative insertion phase from source or load to each open end of resonators can be easily obtained by observing the two-port admittance matrix. Applying the cross coupling from source or load to a proper nonadjacent resonator, a trisection or a quadruplet coupling scheme can be realized with prescribed transmission zeros. More importantly, the proposed trisection can be designed to have a transmission zero on the lower or upper stopband by just adjusting the length of the cross-coupling strip. Using the proposed structure, the conventional time-consuming adjusting procedure to obtain initial physical dimensions of filters is no longer required. In this paper, a fourth-order parallel-coupled filter is used as the basic structure to demonstrate various combinations of transmission zeros. Simulated and measured results are well matched.**

***Index Terms*—Cascade quadruplet (CQ), cascade trisection (CT), cross coupling, mixed cascaded quadruplet and trisection, parallel-coupled filter, transmission zero.**

I. Introduction

HIGH-PERFORMANCE microwave filters are essential circuits in many microwave systems where they serve to pass the wanted signals and suppress unwanted ones in the frequency domain [1]. Cross-coupled filters are attractive since they exhibit highly selective responses, which are required in modern communication systems. Among these cross-coupled filters, the cascade trisection (CT) and cascade quadruplet (CQ) [2]–[7] are two of the most commonly used coupling schemes. Besides the cross-coupled coupling schemes, other coupling topologies such as the doublet, extended doublet, and box section were also found interesting [8], [9] and have been successfully implemented in microstrip form [10], [11]. In brief, all of the mentioned filters are designed to have finite transmission zeros for better selectivity.

Manuscript received February 1, 2008; revised June 6, 2008. First published August 26, 2008; current version published September 5, 2008. This work was supported in part by the National Science Council under Grant NSC95-2221-E-009-042-MY3 and by the Ministry of Education (MoE) under an MoE Aiming for the Top University (ATU) plan grant.

J.-C. Lu and C.-Y. Chang are with the Department of Communication Engineering, National Chiao Tung University, Hsinchu 300, Taiwan, R.O.C. (e-mail: gerching.cm95g@nctu.edu.tw; mhchang@cc.nctu.edu.tw).

C.-K Liao is with the Gemtek Technology Company Ltd., Hsinchu 303, Taiwan, R.O.C. (e-mail: Ching_Liao@gemtek.com.tw).

Color versions of one or more of the figures in this paper are available online at http://ieeexplore.ieee.org.

Digital Object Identifier 10.1109/TMTT.2008.2002226

To design a cross-coupled filter such as the filters in [2]–[6], the following procedures are usually taken. The first step is to synthesize a coupling matrix corresponding to a desired response. Secondly, decide the suitable physical layout of the resonator. Thirdly, adjust distance and orientation of two neighboring resonators two by two to get proper signs and magnitudes of the corresponding coupling coefficients. In this step, Dishal's method [12] is usually used. A detailed description of Dishal's method is given in [2]. Finally, fine tune the entire circuit. The third and final steps are the most tedious and time-consuming steps because, in the third step, they need to generate design curves of coupling and external Q from an electromagnetic (EM) field solver. In the final step, one resonator may have many neighbors so that when adjusting the distance and orientation against one neighbor, the coupling strength with other neighbors may change. Therefore, the iterative adjusting procedure might be required. Another drawback to design the conventional cross-coupled filter is that if one coupling coefficient in the coupling matrix changes sign, the physical layout must be reconfigured. For example, in the case of CT filters of [5], completely different orientations of the resonators must be adopted for a trisection having a lower stopband transmission zero and a trisection having a upper stopband transmission zero because there is one coupling coefficient changed sign. This means that the time-consuming adjusting step described above must be done separately in two cases.

Another interesting cross-coupled filter based on a parallel-coupled filter structure was proposed by Hong and Lancaster [13]. In [13], an extra microstrip line couples the nonadjacent resonators (resonators 1 and 4 in [13]) to produce transmission zeros. By adjusting the length of this extra coupling microstrip line and gaps of the coupling sections, the locations of the transmission zeros can be manipulated. This type of filter has the benefit of simple layout, manageable transmission zeros, and much less time for adjusting layout than conventional cross-coupled filters. However, it has some problems. The extra coupling microstrip line has its own resonant frequencies. If the electrical length of this extra coupling microstrip line is not integer multiples of 180°, spurious responses appear at these resonant frequencies on the lower or upper stopbands. The spurious resonance can seriously degrade the stopband performance of the filter. The situation becomes more severe as the extra coupling line becomes longer. If the electrical length of this extra coupling microstrip line is integer multiples of 180°, it becomes an extra resonant node in the coupling route. This extra resonant node causes the coupling diagram more complexity when synthesizing a proper coupling matrix corresponding to a desired response. One way to solve this problem is to use the source

or load to nonadjacent resonators cross couplings [7]. Unlike [13], the extra coupling line in [7] is directly connected to the source or load so that no self-resonance of this extra coupling line will occur. The filter in [7] can largely simplify the design procedures of a CT filter due to its conventional microstrip parallel-coupled filter structure. The CT filter in [7] introduces cross couplings, $M_{S,2}$ and $M_{L,n-1}$, to generate two trisections so that two independently controllable transmission zeros on the upper stopband are produced. However, the realizable response of the filter in [7] is limited to the CT filter with two upper stopband transmission zeros.

In spite of the cross-coupled schemes, the coupling schemes such as the doublet, extended doublet, and box section are introduced [8], [9]. The main characteristic of these coupling schemes is the ability to shift a transmission zero from one side of the passband to the other by just adjusting the resonant frequencies of resonators in the box portion of the coupling scheme; this is the so-called zero shifting characteristic. Recently, a fourth-order box-section filter proposed by Amari *et al.* [10] and filters with box-like coupling schemes proposed by Liao *et al.* [11] have been successfully implemented using microstrip lines. The drawback of the former is that it needs to use Dishal's method, as described above. The latter used an E-shaped two-mode resonator, namely, even and odd modes, to support corresponding coupling schemes such as the doublet, extended doublet, and box section. Unfortunately, when designing such a two-mode filter, the physical dimensions of the resonators are very sensitive, especially the dimensions of the two-mode resonator. While tuning the filter, carefully adjusting physical parameters of the two-mode resonator is required because some dimensions of the two-mode resonator influence not only the position of the transmission zero, but also the in-band return loss. It means that the designer should spend much time to tune.

In this paper, we propose new cross-coupled filters based on a conventional parallel-coupled filter, and all of the shortcomings described above can be solved. Basically, this newly proposed filter structure takes advantage of Hong's filter [13] and Liao's filter [7]. Fig. 1(a) shows the schematic layout of the proposed filter with a fourth-order filter as an example where the crossing coupling between the source or load and nonadjacent resonators, which are denoted via dotted lines. Its equivalent coupling diagram is shown in Fig. 1(b). The filter has the advantage of using the simple synthesis procedure presented in [14] to serve as the initial design. Although Fig. 1(a) and (b) shows multiple cross-coupling routes from source to nonadjacent resonators, only one of them is chosen in the design procedures. A similar situation occurs in the load end. By observing the relative phase shifts of main and cross-coupled paths between the source or load and one of the nodes of the interested resonator, filters with generalized Chebyshev responses can then be implemented. Applying suitable cross-coupling paths and phases, the proposed filter could be CT, CQ, or a combination of quadruplet and trisection. It is important to note that, in the trisection configuration, the transmission zero can be located on either the lower or upper stopbands by just applying the suitable cross coupling in Fig. 1(a). Therefore, the design procedures of the proposed filter are easy without using of the Dishal's method or the method presented in [2]. Besides, it is more flexible to locate the transmission zeros.

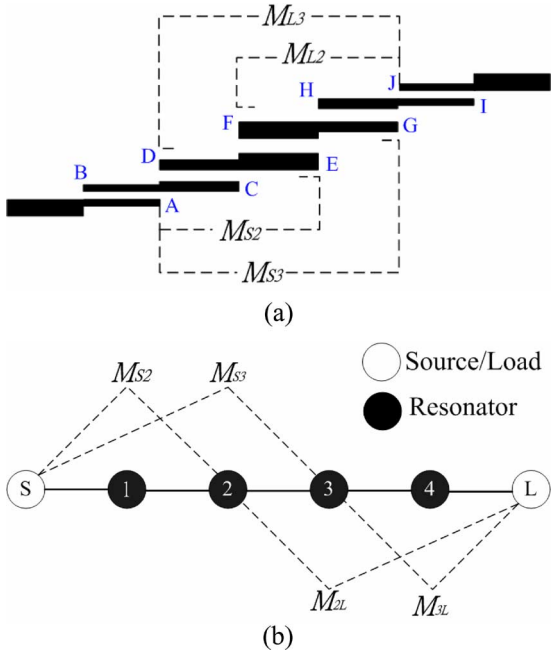

Fig. 1. Cross-coupled parallel coupled filter. (a) Schematic layout. (b) Coupling and routing scheme corresponding to (a).

II. Phase Relationships and Generation of Finite Transmission Zeros

In this section, the purpose is to explore the relative phase shifts of the main coupling path from the source or load to resonators and to apply suitable phase shifts of the cross-coupling paths to generate finite frequency transmission zeros on either the upper or lower stopbands or both of the stopbands. Let us take a fourth-order filter as an example.

In the beginning, the initial design of the proposed filters is based on the conventional parallel-coupled filter presented by Cohn [14]. Fig. 2 shows the lumped-element equivalent circuit of a fourth-order parallel-coupled filter shown in Fig. 1(a). Cross couplings are not introduced at this moment. Here, it should be pointed out that the lumped-element equivalent circuit should include the phase-reversing transformer in every resonator. Although the phase-reversing transformer is often omitted in a conventional parallel-coupled filter due to no effect on the magnitude of filter response, it is, however, very important in the proposed cross-coupled filters. Let us now check phase relationships from the source or load to resonators. In order to observe the relative phase conveniently, we sequentially number the corresponding nodes of Figs. 1(a) and 2 as A–J from source to load. Therefore, the relative phases in the lumped-element circuit model of Fig. 2 can be determined, and all of the insertion phases between node A and nodes B–J in Fig. 1(a) are obtained easily. Consider each box in Fig. 2, which represents an ideal admittance inverter having a constant image admittance and constant phase shift of -90° for all frequencies. Let nodes

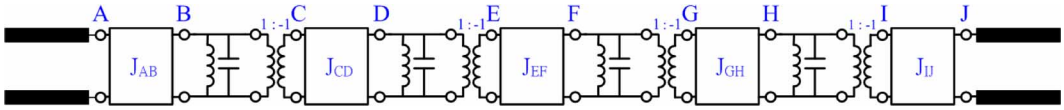

Fig. 2. Equivalent lumped-element circuit of a fourth-order parallel coupled filter.

TABLE I
RELATIVE PHASE SHIFTS OF THE MAIN COUPLING PATH, PROPER PHASES OF THE CROSS-COUPLING PATHS TO GENERATE TRANSMISSION ZEROS, CORRESPONDING RESPONSES, AND DELAY LINE ELECTRICAL LENGTH

	The main coupling path		The cross coupling path		Response	Delay line electrical length	Frequency response predicted
	$f<f_0$	$f>f_0$	$f<f_0$	$f>f_0$			
$Y_{BA}(Y_{IJ})$	-90	-90	Not applicable	Not applicable			
$Y_{CA}(Y_{HJ})$	+90	+90	Not applicable	Not applicable			
$Y_{DA}(Y_{GJ})$	-90	+90	-90	-90	Trisection with a TZ on upper stopband	0^o or 360^o	
$Y_{DA}(Y_{GJ})$	-90	+90	+90	+90	Trisection with a TZ on lower stopband	180^o	
$Y_{EA}(Y_{FJ})$	+90	-90	-90	-90	Trisection with a TZ on lower stopband	0^o or 360^o	
$Y_{EA}(Y_{FJ})$	+90	-90	+90	+90	Trisection with a TZ on upper stopband	180^o	
$Y_{FA}(Y_{EJ})$	-90	-90	+90	+90	Quadruplet	180^o	
$Y_{GA}(Y_{DJ})$	+90	+90	-90	-90	Quadruplet	360^o	
$Y_{HA}(Y_{CJ})$	-90	+90			*		
$Y_{IA}(Y_{BJ})$	+90	-90			*		
$Y_{JA}(Y_{AJ})$	-90	-90			*		

$*$: cross coupling (does not belong to trisection or quadruplet, and is beyond the scope of this paper)

A and B be the input and output ports of the admittance inverter J_{AB}. The matrix element Y_{BA} of the two-port admittance matrix can then be determined. Thus, the phase of Y_{BA} is -90° over both frequency ranges $f < f_0$ and $f > f_0$ where f_0 is the center frequency of the filter. The phase shift of the phase-reversing transformer is also -180° for all frequencies. Consequently, the phase of Y_{CA} is -270° over both frequency ranges $f < f_0$ and $f > f_0$. Next, consider Y_{DA}, where the shunt inductor/capacitor pair, shown in Fig. 2, is a resonator. The phase shift of a resonator at off-resonance frequencies is dependent on whether the frequency is above or below resonance. As $f < f_0$, the admittance of the resonator is inductive and the phase shift should be -90°. Similarly, as $f > f_0$, the admittance of the resonator is capacitive and the phase shift should be $+90^\circ$. As a result, the phase shift of Y_{DA} is -90° when $f < f_0 (-90^\circ - 90^\circ - 180^\circ - 90^\circ = -450^\circ = -90^\circ)$ and $+90^\circ$ when $f > f_0 (-90^\circ + 90^\circ - 180^\circ - 90^\circ = -270^\circ = +90^\circ)$. Following similar analyzing procedures described above, one can observe every relative phase shift between node A and nodes B–J. The phase relationships from the source or load to resonators can be easily observed by using any commercial circuit simulator. Table I summarizes the phase relationships between node A and nodes B–J as $f < f_0$ and $f > f_0$. The method is applicable to any order of a parallel-coupled filter. As a result, the relative phase shifts between node A and nodes B–J in Fig. 1(a) are identical to those of the lumped-element filter in Fig. 2.

Next, the cross-coupling paths will be studied. When a cross-coupling path is applied to node A and another node in the non-adjacent resonator and its phase delay is 180° out-of-phase with the main path, a transmission zero appears.

The trisection coupling scheme in this filter can be formed by adding a cross-coupling path from the source to the second resonator. The two ends of the second resonator corresponds to nodes D and E. Assume the cross-coupling path is applied from the source to node D. Since the phase of the main coupling path Y_{DA} is $+90^\circ$ as $f > f_0$, the phase of the cross-coupling path from the source to node D should be -90° as $f > f_0$ in order to have a upper stopband transmission zero. On the other hand, if the cross-coupling path is applied between the source and node E, the filter can also have a upper stopband transmission zero when the phase of the cross-coupling path Y_{EA} is $+90^\circ$ as $f > f_0$ due to -90° of phase in the main path Y_{EA} as $f > f_0$. In contrast to a upper stopband transmission zero as discussed above, a lower stopband transmission zero

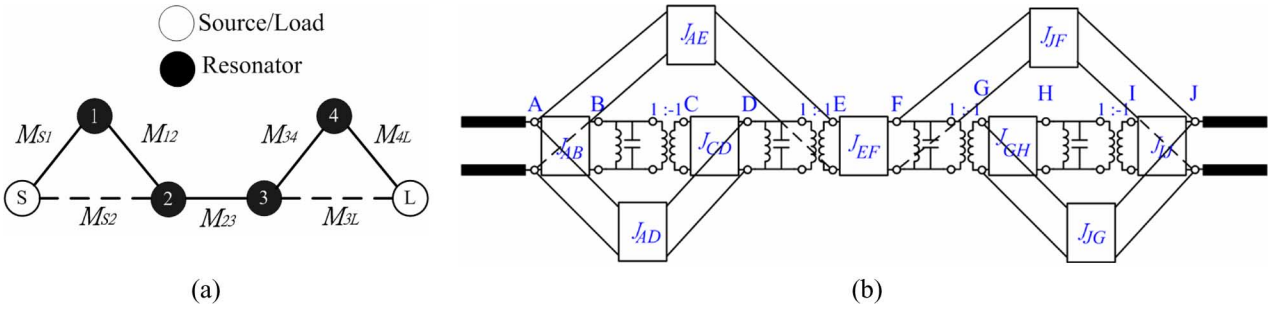

Fig. 3. Cascaded trisection filter. (a) Coupling scheme. (b) Corresponding equivalent lumped-element circuit of a fourth-order parallel coupled filter with cross couplings. Either the inverter $J_{\rm AD}$ or $J_{\rm AE}$ corresponds to M_{S2} and either the inverter $J_{\rm JF}$ or $J_{\rm JG}$ corresponds to M_{3L}.

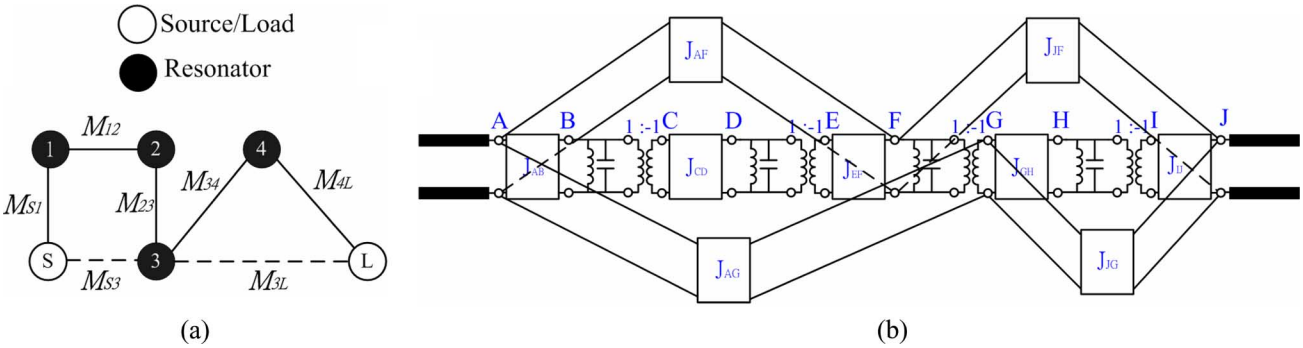

Fig. 4. Mixed cascaded quadruplet and trisection filter. (a) Coupling scheme. (b) Corresponding equivalent lumped-element circuit of a fourth-order parallel coupled filter with cross coupling. Either the inverter $J_{\rm AF}$ or $J_{\rm AG}$ corresponds to M_{S3} and either the inverter $J_{\rm JF}$ or $J_{\rm JG}$ corresponds to M_{3L}.

could also be possible by applying -90° phase shifts of the cross-coupling path $Y_{\rm EA}$ as $f < f_0$ where it is 180° out-of-phase with that of the main path $Y_{\rm EA}$. In spite of the source, the load can also be cross-coupled to the third resonator in Fig. 1(a) to form another trisection.

Another popular coupling scheme is the so-called quadruplet where two transmission zeros, one on the upper stopband and the other on the lower stopband, are generated by applying just one cross-coupling path. The quadruplet cross coupling could be from the source to the third resonator or from the load to the second resonator. Utilizing a similar phase analysis method as a trisection, the phase relationship of the quadruplet coupling scheme can be easily obtained. Let us use the cross-coupling path from source to node G as an example. The phase shift of the main path $Y_{\rm GA}$ is $+90^\circ$ as $f < f_0$ and $f > f_0$. As mentioned above, as long as the phase shift of the cross-coupling path $Y_{\rm GA}$ is -90°, two transmission zeros on both the lower and upper stopbands should appear. Similarly, the quadruplet cross-coupling path could also be formed from the source to node F.

Table I summarizes the phase relationships that may help a designer to judge the relative phase of the main coupling from the source or load to each node and to apply proper phase of the cross coupling to create desired transmission zeros. After the positions of the transmission zeros being qualitatively determined, the proper strength of the cross coupling should be quantitatively determined for a desired specification. A full discussion will be presented in Section III.

III. Cross-Coupling Schemes

Two coupling schemes, namely, the CT and the mixed CQ and CT [15], are possible for our fourth-order examples. Figs. 3(a) and 4(a) show the CT and the mixed CQ and CT coupling schemes, respectively. Although the CT and the mixed CQ and CT coupling schemes have already been proposed in the literature, the microstrip implementation using a parallel-coupled structure is first proposed in this paper. Here, the resonators are represented by dark dots, the source and load by empty dots, the solid lines between resonators indicate the main coupling, and the broken lines indicate the cross coupling.

The lumped-element equivalent circuit of the fourth-order parallel-coupled filter with a CT cross-coupling scheme is shown in Fig. 3(b). Either the inverter $J_{\rm AE}$ or inverter $J_{\rm AD}$ in Fig. 3(b) corresponds to the cross coupling M_{S2} in Fig. 3(a), and similar situation applies to the inverter $J_{\rm JF}$ and the inverter $J_{\rm JG}$. By choosing either $J_{\rm AE}$ or $J_{\rm AD}$ in the source end and either $J_{\rm JF}$ or $J_{\rm JG}$ in the load end, different signs of M_{S2} and M_{3L} can be implemented. Thus, two trisections are formed and each trisection can create a transmission zero on either the lower or upper stopbands. To demonstrate the mentioned properties, three CT filters are discussed as examples.

The first CT filter has the following parameters. Its low-pass prototype is with two transmission zeros at $\Omega = 3$ and $\Omega = -2$, and a maximum in-band return loss of 20 dB. The coupling matrix corresponding to Fig. 3(a) is shown in (1) as follows where the synthesizing techniques in [16] are used:

$$M = \begin{bmatrix} 0 & 0.9024 & -0.4910 & 0 & 0 & 0 \\ 0.9024 & 0.7905 & 0.6581 & 0 & 0 & 0 \\ -0.4910 & 0.6581 & -0.3186 & 0.7285 & 0 & 0 \\ 0 & 0 & 0.7285 & 0.1845 & 0.7990 & 0.3197 \\ 0 & 0 & 0 & 0.7990 & -0.5601 & 0.9763 \\ 0 & 0 & 0 & 0.3197 & 0.9763 & 0 \end{bmatrix}. \quad (1)$$

In the coupling matrix, $M_{S2} = -0.4910$ and $M_{3L} = 0.3197$ are in different signs because one transmission zero on the upper stopband is due to M_{3L} and the other transmission zero on the lower stropband is due to M_{S2}. Since a capacitive coupling provides -90° of phase shift for $f < f_0$ and $f > f_0$, from Table I, an upper stopband transmission zero would be created if a capacitive cross coupling is applied between nodes J and G. Therefore, $J_{\rm JG}$ could be chosen capacitive to realize M_{3L}. Similarly, if a capacitive cross coupling existed between nodes A and E, there would be a finite transmission zero on the lower stopband. Thus, one may choose $J_{\rm AE}$ with capacitive cross coupling to implement M_{S2}. Due to the physical distance of node A to node E, a delay line is introduced to implement cross coupling between nodes A and E. Thanks to this delay line, more flexible design can be achieved. When capacitive coupling in cooperation with a delay line of electrical length 360°, the overall relative phase shift of the cross coupling is still -90° ($-360^\circ - 90^\circ = -90^\circ$) for $f < f_0$ and $f > f_0$. In Table I, relative phase shift of the main coupling path from nodes A to E is 90° on $f < f_0$. Consequently, a finite transmission zero on the lower stopband is generated.

The second CT filter is with two transmission zeros at $\Omega = 3$ and $\Omega = 2$ in the low-pass domain, and with a similar in-band return loss of 20 dB. The synthesized coupling matrix is depicted in (2) as follows:

$$M = \begin{bmatrix} 0 & 0.9167 & 0.4889 & 0 & 0 & 0 \\ 0.9167 & -0.7411 & 0.6714 & 0 & 0 & 0 \\ 0.4889 & 0.6714 & 0.4288 & 0.7357 & 0 & 0 \\ 0 & 0 & 0.7357 & 0.3471 & 0.8118 & 0.3179 \\ 0 & 0 & 0 & 0.8118 & -0.4744 & 0.9891 \\ 0 & 0 & 0 & 0.3179 & 0.9891 & 0 \end{bmatrix}. \tag{2}$$

Note that the sign of M_{S2} changes from negative to positive. Therefore, one may choose $J_{\rm AD}$ as a capacitive cross coupling to achieve $M_{S2} = 0.4889$ and keep $J_{\rm JG}$ unchanged.

The third CT filter has a similar passband return loss, but with two low-pass domain transmission zeros at $\Omega = -3$ and $\Omega = -2$. From the reversal property of the coupling matrix, the absolute values of the matrix elements should equal to those of (2) and M_{11}, M_{22}, M_{33}, M_{44}, M_{S2}, M_{2S}, and M_{3L}, and M_{L3} should change sign [17]. The coupling matrix is shown in (3) as follows:

$$M = \begin{bmatrix} 0 & 0.9167 & -0.4889 & 0 & 0 & 0 \\ 0.9167 & 0.7411 & 0.6714 & 0 & 0 & 0 \\ -0.4889 & 0.6714 & -0.4288 & 0.7357 & 0 & 0 \\ 0 & 0 & 0.7357 & -0.3471 & 0.8118 & -0.3179 \\ 0 & 0 & 0 & 0.8118 & 0.4744 & 0.9891 \\ 0 & 0 & 0 & -0.3179 & 0.9891 & 0 \end{bmatrix}. \tag{3}$$

Thus, we may choose $J_{\rm AE}$ with capacitive cross coupling to achieve $M_{S2} = -0.4889$ and choose $J_{\rm JF}$ with capacitive cross coupling to achieve $M_{3L} = -0.3179$. Again, due to physical distances of nodes A–E and nodes J–F, two capacitive cross coupling in cooperation with two delay lines of electrical length 360° implement the desired $J_{\rm AE}$ and $J_{\rm JF}$. The low-pass domain responses of the three CT filters are shown in Fig. 5.

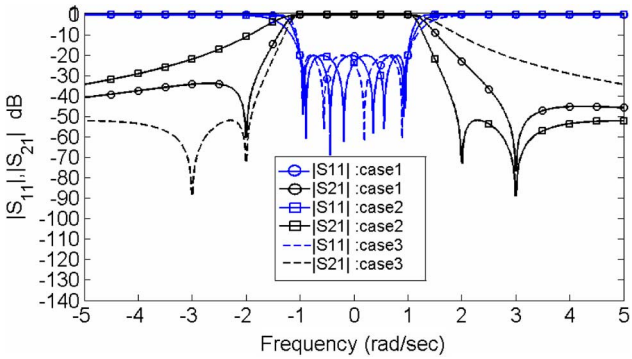

Fig. 5. Low-pass responses of the three CT filters with all in-band return loss of 20 dB. Case 1: normalized transmission zeros at $\Omega = 3$ and $\Omega = -2$. Case 2: normalized transmission zeros at $\Omega = 3$ and $\Omega = 2$. Case 3: normalized transmission zeros at $\Omega = -3$ and $\Omega = -2$.

Fig. 4(a) shows the coupling scheme of the fourth-order mixed CQ and CT filter. This topology is particularly interesting because the quadruplet part can produce a pair of transmission zeros on both sides of the stopband, and the trisection part could generate another transmission zero on whatever location we want. Fig. 4(b) is the lumped-element equivalent circuit of a fourth-order parallel-coupled filter with the mixed CQ and CT cross coupling where nodes A–J in Fig. 4(b) correspond to similar nodes in Fig. 1(a). Again, either the inverter $J_{\rm AF}$ or $J_{\rm AG}$ in Fig. 4(b) can implement the cross coupling M_{S3} in Fig. 4(a), and either the inverter $J_{\rm JF}$ or $J_{\rm JG}$ in Fig. 4(b) can realize the cross coupling M_{3L} in Fig. 4(a). Let us consider the quadruplet portion of the mixed CQ and CT filter first. Suppose that a capacitive coupling gap is applied at node F. From Table I, a delay line with an electrical length of 180° should be involved between the source and capacitive coupling gap (node F) to create proper phases of the cross coupling ($-180^\circ - 90^\circ = -270^\circ = +90^\circ$ for $f < f_0$ and $f > f_0$) so that a pair of transmission zeros could be created on both sides of the stopband. Oppositely, if the capacitive gap is applied at node G to realize the cross coupling, the inserted delay line between nodes A and G should be 360°. Considering the layout, a capacitive gap applied to node F is preferable. The trisection portion of the mixed CQ and CT filter is similar to that of the CT filter discussed earlier. If a finite transmission zero on the upper stopband is desired, one may choose the capacitive inverter $J_{\rm JG}$ in Fig. 4(b) to implement the cross coupling M_{3L} in Fig. 4(a). Contrarily, if a finite transmission zero on the lower stopband is desired, the cross coupling M_{3L} in Fig. 4(a) could be realized by the capacitive inverter $J_{\rm JF}$ in Fig. 4(b). To reach nodes J–F, a delay line with an electrical length of 360° should be involved. The delay line and the coupling gap form an overall phase shift of -90° ($-360^\circ - 90^\circ = -90^\circ$ for $f < f_0$ and $f > f_0$). In brief, a mixed CQ and CT filter can have not only a pair of transmission zeros on both sides of the stopband, but also another transmission zero on either the upper or lower stopbands.

IV. Filter Design Examples

Since a mixed CQ and CT filter contains two types of cross couplings and is more general than a CT filter, two fourth-order

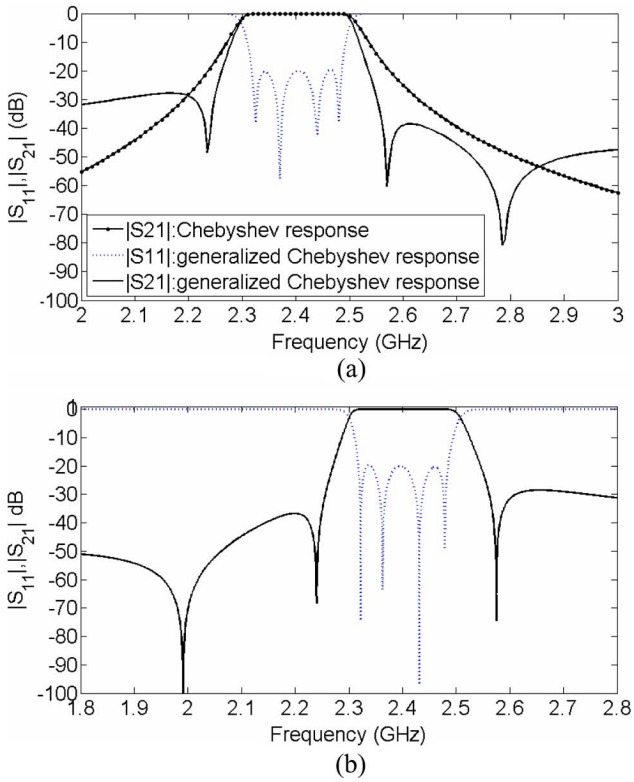

Fig. 6. Ideal responses of the two CQT filters. (a) Bandpass response corresponding to (4) with a typical Chebyshev response as a reference. (b) Bandpass response corresponding to (5).

parallel-coupled filters with mixed CQ and CT cross coupling are chosen as examples in this section to demonstrate the feasibility of the proposed structures. A 0.508-mm-thick Rogers RO4003 substrate with a relative dielectric constant of 3.58 and a loss tangent of 0.0021 is used to implement these mixed CQ and CT filters.

The first mixed CQ and CT filter is designed to have a pair of real frequency transmission zeros at normalized frequencies of $\Omega = \pm 2$, a real frequency transmission zero at a normalized frequency of $\Omega = 4$ in the low-pass domain, and a passband return loss of 20 dB. Fig. 4(a) shows the coupling scheme of the mixed CQ and CT filter. Equation (4) is the synthesized coupling matrix

$$M = \begin{bmatrix} 0 & 1.0039 & 0 & -0.1998 & 0 & 0 \\ 1.0039 & 0.0111 & 1.0020 & 0 & 0 & 0 \\ 0 & 1.0020 & 0.0317 & 0.5879 & 0 & 0 \\ -0.1998 & 0 & 0.5879 & 0.1788 & 0.8409 & 0.2136 \\ 0 & 0 & 0 & 0.8409 & -0.3487 & 1.0010 \\ 0 & 0 & 0 & 0.2136 & 1.0010 & 0 \end{bmatrix}. \tag{4}$$

The filter is then transformed from the low-pass domain to the bandpass domain with the center frequency of $f_0 = 2.4$ GHz and the fractional bandwidth of 7%. The response after transformation is depicted in Fig. 6(a).

The design procedures are described briefly as follows.

First, calculate the initial design by applying Cohn's analytical synthesis method [14] to realize the inline part of the coupling matrix. For our fourth-order filter, the inline part coupling elements are M_{S1}, M_{12}, M_{23}, M_{34}, and M_{4L}. That is to get the J-inverter values from these coupling elements, and using Cohn's formula to get the even- and odd-mode impedances of each parallel-coupled section corresponding to the J-inverter values. Note that no cross couplings are introduced at this moment so that the electrical length of each parallel-coupled section is 90°. After this, the layout can be modified according to [18] in that each resonator's vertical position can be vertically flipped to make cross couplings easy to apply. In this example, the source feeding line and the first resonator is vertically flipped as is the load feeding line and the last resonator such that the nodes to implement the cross coupling of M_{S3} and M_{3L} can be accessed. The parallel-coupled filter portion in Fig. 7(a) depicts the modification of the layout.

Secondly, if nodes A and F are chosen to implement the cross coupling of $M_{S3} = -0.1998$, a delay line with an electrical length of 180° in cooperation with a capacitive coupling should be used. The reason to use the 180° delay line has been described in Section III. The initial length of the capacitive coupling gap is obtained by a circuit simulator such as Agilent's Advanced Design System (ADS) [19]. For simplifying the layout, the width of the delay line is fixed to be 0.254 mm and the coupling gap between the delay line and resonator 3 is also fixed to be 0.254 mm. Now, resonator 3 is coupled to the source through the delay line. The electrical length of the delay line is adjusted to be 180° at the center frequency. The coupling length can be easily adjusted by using the three coupled-line model in ADS where the linewidths and gapwidths remain unchanged since tuning of the coupling length in the circuit simulator can almost be real time. The initial coupling length can be quickly obtained as 3.937 mm. Therefore, the physical layout of the quadruplet portion of the first mixed CQ and CT filter is obtained.

Finally, the trisection portion of this mixed CQ and CT filter is the same as that of CT filter described in [7], where an upper stopband transmission zero can be easily obtained. As with the similar method proposed in [7], a coupling/shielding line is adopted here at node J of the output feed line. This would be the simplest way to implement M_{3L} where a transmission zero at a normalized frequency of $\Omega = 4$ could be created. Finally, fine tuning might be required using an EM simulator. After fine tuning of the entire circuit with the commercial EM simulator Sonnet [20], all physical dimensions of the filter are obtained. The circuit layout and the detailed dimensions are shown in Fig. 7(a) and in Table II, respectively, and a photograph of the filter is depicted in Fig. 8(a).

The second mixed CQ and CT filter is designed to have a pair of real frequency transmission zeros at normalized frequencies of $\Omega = \pm 2$, a real frequency transmission zero at a normalized frequency of $\Omega = -5$ in the low-pass domain, and a passband return loss of 20 dB. The synthesized coupling matrix is shown in (5) as follows:

$$M = \begin{bmatrix} 0 & 1.0041 & 0 & -0.1986 & 0 & 0 \\ 1.0041 & -0.0090 & 1.0019 & 0 & 0 & 0 \\ 0 & 1.0019 & -0.0250 & 0.5871 & 0 & 0 \\ -0.1986 & 0 & 0.5871 & -0.1435 & 0.8579 & -0.1700 \\ 0 & 0 & 0 & 0.8579 & 0.2785 & 1.0094 \\ 0 & 0 & 0 & -0.1700 & 1.0094 & 0 \end{bmatrix}. \tag{5}$$

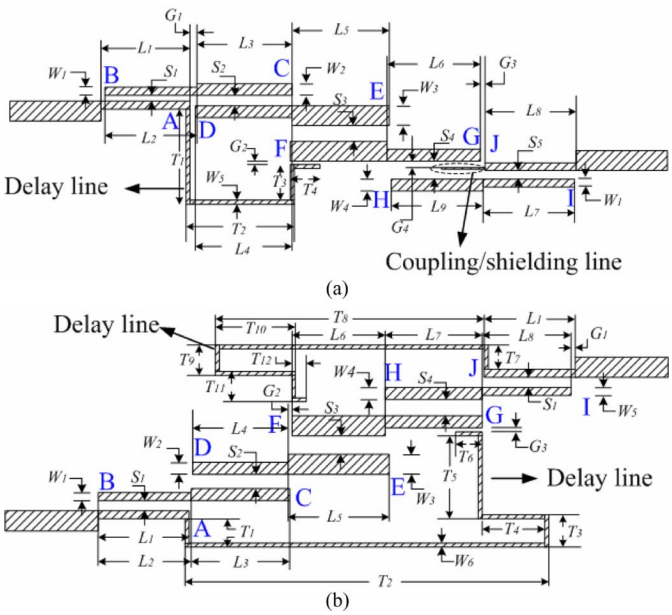

Fig. 7. Circuit layouts of the proposed filters. (a) First designed mixed cascaded quadruplet and trisection filter. The length and linewidth of coupling/shielding line are 4.318 and 0.177 mm, respectively. (b) Second designed mixed cascaded quadruplet and trisection filter.

TABLE II
PHYSICAL DIMENSIONS OF THE TWO PROPOSED FILTERS

The dimensions of the first designed mixed cascaded quadruplet and trisection filter corresponding to layout in Fig. 7(a) (in mm)						
L_1	L_2	L_3	L_4	L_5	L_6	L_7
18.999	19.181	17.779	17.830	19.253	17.729	19.253
L_8	L_9	S_1	S_2	S_3	S_4	S_5
19.075	17.729	0.177	0.508	0.965	0.558	0.177
W_1	W_2	W_3	W_4	W_5	G_1	G_2
0.660	1.143	1.092	1.193	0.254	0.254	0.254
G_3	G_4	T_1	T_2	T_3	T_4	
0.203	0.203	9.652	18.288	5.181	3.810	
The dimensions of the second designed mixed cascaded quadruplet and trisection filter corresponding to layout in Fig. 7(b) (in mm)						
L_1	L_2	L_3	L_4	L_5	L_6	L_7
19.100	19.253	19.805	17.754	18.872	18.669	17.754
L_8	S_1	S_2	S_3	S_4	W_1	W_2
19.050	0.177	0.508	0.939	0.558	0.736	1.270
W_3	W_4	W_5	W_6	G_1	G_2	G_3
1.143	1.320	0.711	0.254	0.203	0.076	0.254
T_1	T_2	T_3	T_4	T_5	T_6	T_7
3.733	60.960	2.794	6.045	5.588	3.810	3.632
T_8	T_9	T_{10}	T_{11}	T_{12}		
52.628	2.794	16.281	3.276	1.143		

Similarly, the low-pass prototype is transformed into the bandpass domain with the center frequency of $f_0 = 2.4$ GHz and the fractional bandwidth of 7%. The transformed bandpass response is depicted in Fig. 6(b). The initial dimensions of the parallel-coupled portion of the filter are calculated by the analytical method as described in the first filter. Again, let us look at the quadruplet portion of the filter first. This time, nodes A and G in Fig. 4(b) are chosen to implement the cross coupling between the source and resonator 3. From (5), the synthesized cross-coupling value should be $M_{S3} = -0.1986$. Therefore,

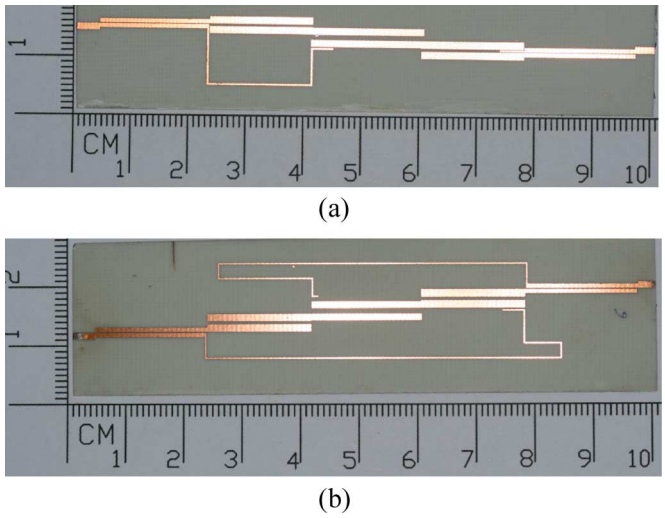

Fig. 8. Layouts of the implemented filters. (a) First designed filter. (b) Second designed filter.

a delay line with an electrical length of 360° in cooperation with a capacitive coupling would be appropriate to implement M_{S3}. Again, the width of the delay line is fixed to be 0.254 mm and the coupling gap is also fixed to be 0.254 mm. The initial coupling length of 3.937 mm is then obtained by the circuit simulator. Finally, let us look at the trisection portion of the filter. Now, nodes J and F are chosen to implement the cross coupling between resonator 3 and the load. A delay line with an electrical length of 360° in cooperation with a capacitive cross coupling could realize the cross coupling with the correct phase and amplitude. The strip width of the delay line is still fixed to be 0.254 mm. Different from the former, the capacitive coupling gap is now fixed to be 0.762 mm in this case. Similarly, the initial coupling length of 1.143 mm is obtained by the circuit simulator. As with the first filter, the initial physical dimensions of the second filter can be obtained from ADS, and then EM simulation to fine tune the physical dimensions might be required. After fine tuning with the commercial EM simulator Sonnet, the circuit layout and the detailed dimensions are shown in Fig. 7(b) and Table II, respectively. The circuit photograph is shown in Fig. 8(b).

V. RESULTS AND DISCUSSION

Shown in Fig. 9(a) are the measured and simulated performances of the first mixed CQ and CT filter. The measured center frequency, fractional bandwidth, and in-band insertion loss are 2.4 GHz, 7%, and 1.8 dB, respectively, which are in good agreement with the simulated results. The two transmission zeros contributed by the quadruplet part are at 2.23 and 2.585 GHz, and also agree well with the simulation. The third transmission zero is at 2.82 GHz, and the little deviation might come from the much weaker and more sensitive coupling between the coupling/shielding line and resonator 3 than that of the quadruplet portion.

Fig. 9(b) shows the measured performance of the second mixed CQ and CT filter. Again, the measured center frequency, fractional bandwidth, in-band insertion loss, and two transmission zeros contributed by the quadruplet part of the filter are

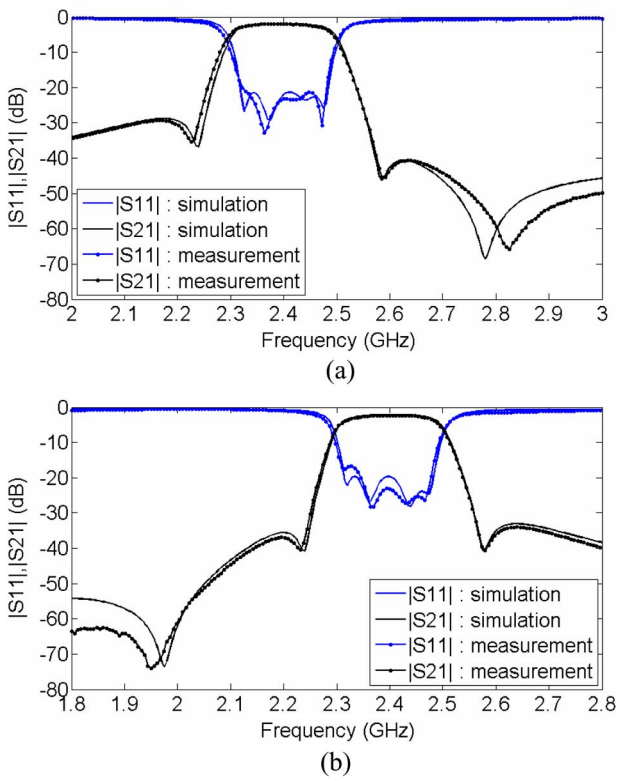

Fig. 9. Measured and simulated performances of the two implemented filters. (a) First designed filter. (b) Second designed filter.

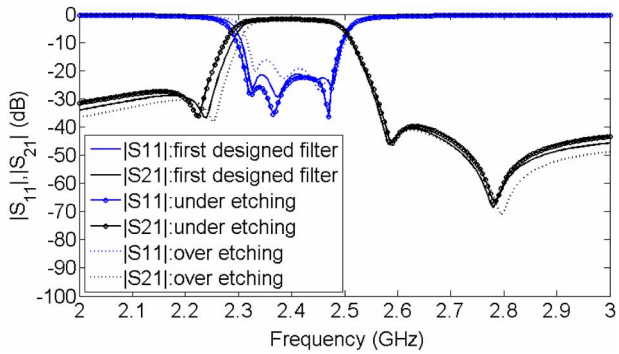

Fig. 10. Sensitivity analysis of the first mixed CQ and CT filter for under etching of 0.0508 mm (2 mil) and over etching of 0.0508 mm, respectively.

also in good agreement with the simulated results. The third transmission zero similarly shows a little frequency drift to lower frequency compared with the simulation.

The sensitivity analysis of the proposed filters to manufacturing tolerances can be performed in two conditions. One is over etching 0.0508 mm (2 mil), the other is under etching 0.0508 mm (2 mil). Take the first mixed CQ and CT filter as an example and simulate it in two conditions using the EM simulator Sonnet. The simulated responses are shown in Fig. 10. It is found that the proposed cross-coupled filters are not very sensitive to the manufacturing tolerances.

Another concern is that as the finite transmission zeros get closer to the passband, the values of the cross coupling should be higher and some dimensions of the circuit layouts must change.

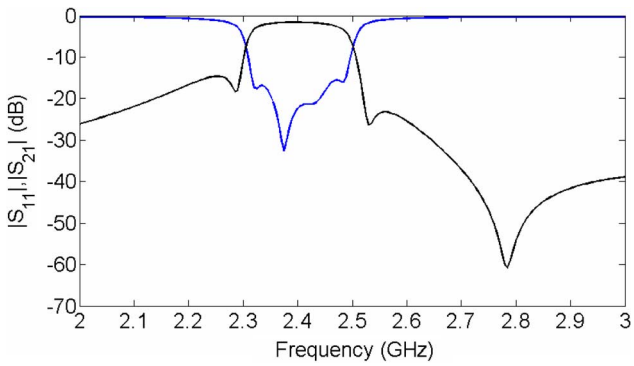

Fig. 11. Simulated performances of the first mixed cascaded quadruplet and trisection filter with finite transmission zeros at $\Omega = \pm 1.4, 4$.

On the other hand, for a highly asymmetrical response with the transmission zeros very close to the passband, the lengths of the resonators should be modified because the trisection portion of the filter becomes highly asynchronously tuned. How close the transmission zeros to the passband can be before the layout becomes impractical for fabrication or the design becomes very difficult to estimate.

The situation can be summarized in two cases. The first case is the pair of quadruplet transmission zeros very close to the passband, and the second case is the trisection transmission zero very close to the passband. Let us take the first mixed CQ and CT filter in Fig. 7(a) as an example to study these two cases.

In the first case, as the pair of quadruplet transmission zeros move from $\Omega = \pm 2$ to $\Omega = \pm 1.4$ in the low-pass domain, the corresponding coupling matrix M is obtained as

$$M = \begin{bmatrix} 0 & 0.8849 & 0 & -0.4935 & 0 & 0 \\ 0.8849 & -0.0108 & 1.0967 & 0 & 0 & 0 \\ 0 & 1.0967 & 0.0306 & 0.3780 & 0 & 0 \\ -0.4935 & 0 & 0.3780 & 0.1746 & 0.8488 & 0.2054 \\ 0 & 0 & 0 & 0.8488 & -0.3212 & 0.9940 \\ 0 & 0 & 0 & 0.2054 & 0.9940 & 0 \end{bmatrix}. \quad (6)$$

Following the design procedures described above, the EM simulated response and the detailed dimensions are then shown in Fig. 11 and Table III, respectively. It is found that the coupled section length T_4 of the delay line is increased from 3.81 to 8.382 mm to achieve the proper value of M_{S2}. It is also reasonable that some dimensions such as S_1, S_3, and G_2 in Fig. 7(a) are changed corresponding to the variation of matrix elements. It can be observed in Table III that the layout dimensions are still good for the printed circuit board process. It seems that the cross-coupling strength could be implemented much stronger. However, it must be noted that increasing the value of T_4 causes much higher unwanted coupling of M_{S2}. It may cause the transmission zeros to drift slightly. The drift of transmission zeros becomes worse as the cross coupling becomes stronger.

In the second case, as the trisection transmission zero moves from $\Omega = 4$ to $\Omega = 1.5$ and the pair of quadruplet transmission zeros move from $\Omega = \pm 2$ to $\Omega = \pm 3$ in the low-pass domain, the coupling matrix is obtained as

TABLE III
DIMENSIONS OF THE FIRST DESIGNED MIXED CASCADED QUADRUPLET AND TRISECTION FILTER WITH FINITE TRANSMISSION ZEROS CLOSER TO THE PASSBAND

The filter with finite transmission zeros at Ω=±1.4 , 4. The length and line width of the coupling/shielding line are 4.318 mm and 0.177 mm, respectively						
L_1	L_2	L_3	L_4	L_5	L_6	L_7
18.923	19.227	17.907	17.78	19.431	17.627	19.177
L_8	L_9	S_1	S_2	S_3	S_4	S_5
19.075	17.627	0.228	0.482	1.194	0.584	0.203
W_1	W_2	W_3	W_4	W_5	G_1	G_2
0.660	1.066	1.092	1.193	0.254	0.330	0.178
G_3	G_4	T_1	T_2	T_3	T_4	
0.305	0.229	7.493	18.262	3.987	8.382	
The filter with finite transmission zeros at Ω=+1.5, ±3. The length and line width of the coupling/shielding line are 9.144 mm and 0.127 mm, respectively.						
L_1	L_2	L_3	L_4	L_5	L_6	L_7
18.186	18.135	19.304	19.304	17.830	19.075	18.110
L_8	L_9	S_1	S_2	S_3	S_4	S_5
18.542	18.618	0.152	0.584	0.711	1.066	0.228
W_1	W_2	W_3	W_4	W_5	G_1	G_2
0.711	1.168	1.194	0.889	0.254	0.330	0.508
G_3	G_4	T_1	T_2	T_3	T_4	
0.355	0.127	9.906	19.685	6.527	3.81	

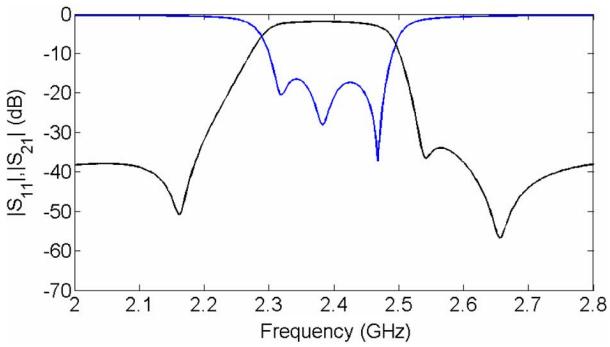

Fig. 12. Simulated performances of the first mixed cascaded quadruplet and trisection filter with finite transmission zeros at $\Omega = +1.5, \pm 3$.

$$M = \begin{bmatrix} 0 & 1.0214 & 0 & -0.0955 & 0 & 0 \\ 1.0214 & 0.0453 & 0.9545 & 0 & 0 & 0 \\ 0 & 0.9545 & 0.1102 & 0.6936 & 0 & 0 \\ -0.0955 & 0 & 0.6936 & 0.4277 & 0.4560 & 0.6541 \\ 0 & 0 & 0 & 0.4560 & -0.9655 & 0.7903 \\ 0 & 0 & 0 & 0.2054 & 0.7903 & 0 \end{bmatrix}. \tag{7}$$

As can be seen in (7), the highest absolute value of the diagonal elements is $M_{44} = -0.9655$. The high value of M_{44} means that the length of resonator 4 should be largely modified. If the length of the coupled-line section changes too much, the main coupling strength may change such that the dimensions need to be adjusted. For the highly asymmetric trisection transmission zero closer to the passband, the width and length of the coupling/shielding line also become narrower and longer, respectively, and the gap between the coupling/shielding line and the third resonator shown in Fig. 7(a) becomes too narrow to be realized. In this case, the iteration process should be adopted. Nevertheless, this process can be done in the circuit simulator ADS so that it is not very time consuming to get the initial layout. In this condition of the highly asymmetric response, the EM simulation to fine tune the physical dimensions must then be required. After fine tuning with the commercial EM simulator Sonnet, the EM simulated response and the detailed dimensions are shown in Fig. 12 and Table III, respectively. It is found that the length and width of the coupling/shielding line are 9.144 and 0.127 mm, respectively. The gap G_4 is 0.127 mm. The manufacturing process can still support the narrow width and small gap.

VI. CONCLUSIONS

Parallel-coupled filters with generalized Chebyshev responses have been presented in this paper. Due to the well-known analytical design method, a good initial design can be quickly obtained. The arbitrarily located transmission zeros have been fully discussed by observing the relative phase shifts of the lumped-element equivalent circuit of the parallel-coupled filter. With this approach, it is easy to design the parallel-coupled filter with a CT, a CQ, or a mixed cascaded quadruplet and trisection response. Two mixed CQ and CT filters have been designed and implemented and the measured results have shown good agreement with simulation results. The newly proposed filter structure has shown properties of insensitive layout, flexible responses, good performance, and quick design procedures.

REFERENCES

[1] I. Hunter, *Theory and Design of Microwave Filters*. London, U.K.: IEE Press, 2001.
[2] J. S. Hong and M. J. Lancaster, *Microstrip Filters for RF/Microwave Applications*. New York: Wiley, 2001.
[3] J. S. Hong and M. J. Lancaster, "Couplings of microstrip square open-loop resonators for cross-coupled planar microwave filters," *IEEE Trans. Microw. Theory Tech.*, vol. 44, no. 12, pp. 2099–2108, Dec. 1996.
[4] C. K. Liao and C. Y. Chang, "A novel five-pole microstrip cascade quadruplet filter," in *Proc. Asia–Pacific Microw. Conf.*, Suzhou, China, 2005, pp. 433–436.
[5] C. C. Yang and C. Y. Chang, "Microstrip cascade trisection filter," *IEEE Microw. Guided Wave Lett.*, vol. 9, pp. 271–273, July 1999.
[6] C. Y. Chang and C. C. Chen, "A novel coupling structure suitable for cross-coupled filters with folded quarter-wave resonators," *IEEE Microw. Wireless Compon. Lett.*, vol. 13, no. 12, pp. 517–519, Dec. 2003.
[7] C. K. Liao and C. Y. Chang, "Modified parallel-coupled filter with two independently controllable upper stopband transmission zeros," *IEEE Microw. Wireless Compon. Lett.*, vol. 15, no. 12, pp. 841–843, Dec. 2005.
[8] R. J. Cameron, A. R. Harish, and C. J. Radcliffe, "Synthesis of advanced microwave filters without diagonal cross-couplings," *IEEE Trans. Microw. Theory Tech.*, vol. 50, no. 12, pp. 2862–2872, Dec. 2002.
[9] U. Rosenberg and S. Amari, "Novel coupling schemes for microwave resonator filters," *IEEE Trans. Microw. Theory Tech.*, vol. 50, no. 12, pp. 2896–2902, Dec. 2002.
[10] S. Amari, G. Tadeson, J. Cihlar, R. Wu, and U. Rosenberg, "Pseudo-elliptic microstrip line filters with zero-shifting properties," *IEEE Microw. Wireless Compon. Lett.*, vol. 14, no. 7, pp. 346–348, Jul. 2004.
[11] C. K. Liao, P. L. Chi, and C. Y. Chang, "Microstrip realization of generalized Chebyshev filters with box-like coupling schemes," *IEEE Trans. Microw. Theory Tech.*, vol. 53, no. 1, pp. 147–153, Jan. 2007.
[12] M. Dishal, "Alignment and adjustment of synchronously tuned multiple-resonator-circuit filters," *Proc. IRE*, vol. 39, no. 11, pp. 1448–1455, Nov. 1951.
[13] J. S. Hong and M. J. Lancaster, "Transmission line filters with advanced filtering characteristics," in *IEEE MTT-S Int. Microw. Symp. Dig.*, 2000, pp. 319–322.

[14] S. B. Cohn, "Parallel-coupled transmission-line-resonator filters," *IRE Trans. Microw. Theory Tech.*, vol. MTT-6, no. 4, pp. 223–231, Apr. 1958.
[15] J. S. Hong, "Computer-aided synthesis of mixed cascaded quadruplet and trisection (CQT) filters," in *Proc. 31st Eur. Microw. Conf.*, London, U.K., Sep. 2001, vol. 3, pp. 5–8.
[16] R. J. Cameron, "Advanced coupling matrix synthesis techniques for microwave filters," *IEEE Trans. Microw. Theory Tech.*, vol. 51, no. 1, pp. 1–10, Jan. 2003.
[17] R. J. Cameron, J. C. Faugere, and F. Seyfert, "Coupling matrix synthesis for a new class of microwave filter configuration," in *IEEE MTT-S Int. Microw. Symp. Dig.*, 2005, pp. 119–122.
[18] C.-Y. Chang and T. Itoh, "A modified parallel-coupled filter structure that improves the upper stopband rejection and response symmetry," *IEEE Trans. Microw. Theory Tech.*, vol. 39, no. 2, pp. 310–314, Feb. 1991.
[19] Advanced Design System (ADS). ver. 2003C, Agilent Technol., Santa Rosa, CA, 2003.
[20] *"EM User's Manual,"* Sonnet Softw. Inc., Liverpool, NY, 2004.

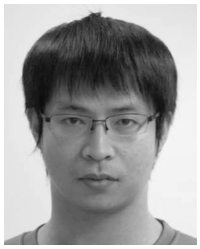

Jhe-Ching Lu was born in Kaohsiung, Taiwan, R.O.C., on May 18, 1982. He received the B.S. degree in electrical engineering from National Sun Yat-Sen University, Kaohsiung, Taiwan, R.O.C., in 2004, the M.S. degree in communication engineering from National Chiao-Tung University, Hsinchu, Taiwan, R.O.C., in 2006, and is currently working toward the Ph.D. degree in communication engineering at the National Chiao-Tung University.

His research interests are microwave filter design and coupler design.

Ching-Ku Liao was born in Taiwan, R.O.C., on October 16, 1978. He received the B.S. degree in electrophysics and M.S. and Ph.D. degrees in communication engineering from National Chiao-Tung University, Hsinchu, Taiwan, R.O.C., in 2001, 2003, and 2007, respectively.

From 2006 to 2007, he was a Visiting Researcher with the University of Florida, sponsored by the National Science Council's Graduate Student Study Abroad Program (GSSAP). He is currently a Senior Engineer with the Gemtek Technology Company Ltd., Hsinchu, Taiwan, R.O.C. His research interests include the analysis and design of microwave and millimeter-wave circuits.

Dr. Liao is a member of Phi Tau Phi.

Chi-Yang Chang (S'88–M'95) was born in Taipei, Taiwan, R.O.C., on December 20, 1954. He received the B.S. degree in physics and M.S. degree in electrical engineering from National Taiwan University, Taipei, Taiwan, R.O.C., in 1977 and 1982, respectively, and the Ph.D. degree in electrical engineering from the University of Texas at Austin, in 1990.

From 1979 to 1980, he was with the Department of Physics, National Taiwan University, as a Teaching Assistant. From 1982 to 1988, he was with the Chung-Shan Institute of Science and Technology (CSIST), as an Associate Researcher, where he was in charge of development of microwave integrated circuits (MICs), microwave subsystems, and millimeter-wave waveguide E-plane circuits. From 1990 to 1995, he was an Associate Researcher with CSIST, where he was in charge of the development of uniplanar circuits, ultra-broadband circuits, and millimeter-wave planar circuits. In 1995, he joined the faculty of the Department of Communication Engineering, National Chiao-Tung University, Hsinchu, Taiwan, R.O.C., as an Associate Professor and became a Professor in 2002. His research interests include microwave and millimeter-wave passive and active circuit design, planar miniaturized filter design, and monolithic-microwave integrated-circuit (MMIC) design.